Original Research

Intracellular Delivery by Shape Anisotropic Magnetic Particle–Induced Cell Membrane Cuts

Journal of Laboratory Automation
2016, Vol. 21(4) 548–556

DOI: 10.1177/2211068216630743
jala.sagepub.com
SAGE

Ming-Yu Lin[1], Yi-Chien Wu[2], Ji-Ann Lee[3], Kuan-Wen Tung[2], Jessica Zhou[2], Michael A. Teitell[4–6], J. Andrew Yeh[1], and Pei Yu Chiou[2,5,6]

Abstract

Introducing functional macromolecules into a variety of living cells is challenging but important for biology research and cell-based therapies. We report a novel cell delivery platform based on rotating shape anisotropic magnetic particles (SAMPs), which make very small cuts on cell membranes for macromolecule delivery with high efficiency and high survivability. SAMP delivery is performed by placing commercially available nickel powder onto cells grown in standard cell culture dishes. Application of a uniform magnetic field causes the magnetic particles to rotate because of mechanical torques induced by shape anisotropic magnetization. Cells touching these rotating particles are nicked, which generates transient membrane pores that enable the delivery of macromolecules into the cytosol of cells. Calcein dye, 3 and 40 kDa dextran polymers, a green fluorescence protein (GFP) plasmid, siRNA, and an enzyme (β-lactamase) were successfully delivered into HeLa cells, primary normal human dermal fibroblasts (NHDFs), and mouse cortical neurons that can be difficult to transfect. The SAMP approach offers several advantages, including easy implementation, low cost, high throughput, and efficient delivery of a broad range of macromolecules. Collectively, SAMP delivery has great potential for a broad range of academic and industrial applications.

Keywords

intracellular delivery, gene therapy, siRNA, enzyme, mouse cortical neurons

Introduction

Efficient delivery of exogenous functional molecules into cells is required in numerous biomedical applications. For example, intracellular delivery of enzymes is a very promising therapeutic approach for genetic diseases because of their catalytic activity and specificity.[1,2] DNA and RNA transfection is indispensible for fundamental biology studies[3,4] and gene therapy.[5–7] Delivery of functional nanoparticles such as conjugation with quantum dots enables real-time fluorescence tracking and imaging.[8,9]

Current delivery approaches are versatile, and each has it own unique advantages and limitations. For example, viral-based approaches can provide high transfer efficiency but are restricted to kilobase-sized nucleic acids with potential immunologic concerns.[10,11] Chemical methods that utilize lipids, cationic polymers, or insoluble precipitates vary in delivery efficiency and are highly cell type dependent.[12,13] Physical approaches, such as electroporation, optoporation, and magnetofection, have been developed.[14–16] However, cell viability, efficiency, setup cost, conjugation of molecules onto magnetic nanoparticles, and cytotoxicity from iron oxide nanoparticles are current obstacles.[17–20] A low-cost, high-efficiency, and high-throughput method for intracellular delivery remains highly desirable.

[1]Instrument Technology Research Center, National Applied Research Laboratories, Hsinchu, Taiwan
[2]Mechanical and Aerospace Engineering Department, University of California at Los Angeles, Los Angeles, CA, USA
[3]Department of Biological Chemistry, University of California at Los Angeles, Los Angeles, CA, USA
[4]Department of Pathology and Laboratory Medicine, David Geffen School of Medicine, University of California at Los Angeles, Los Angeles, CA, USA
[5]Department of Bioengineering, University of California at Los Angeles, Los Angeles, CA, USA
[6]California NanoSystems Institute (CNSI), University of California at Los Angeles, Los Angeles, CA, USA

Received Dec 4, 2015.

Supplementary material for this article is available on the *Journal of Laboratory Automation* Web site at http://jla.sagepub.com/supplemental.

Corresponding Author:
Pei Yu Chiou, California NanoSystems Institute (CNSI), University of California at Los Angeles, 37-138 Engineering IV, 420 Westwood Plaza, Los Angeles, CA, USA.
Email: pychiou@seas.ucla.edu

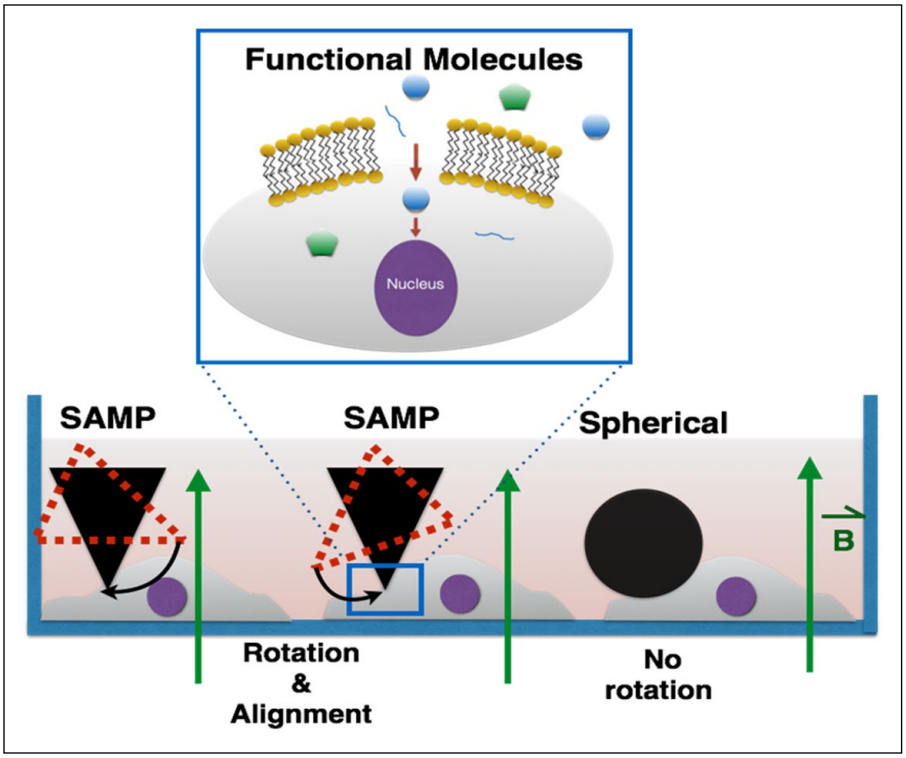

Figure 1. Principle of intracellular delivery using the SAMP method. A uniform magnetic field magnetizes SAMPs and aligns their easy axes with the applied field. Cells touching SAMPs are scratched and open transient membrane pores for cytosolic delivery. Magnetic particles with symmetric shapes do not rotate under a uniform magnetic field since there is no direction preference of magnetization (see **Suppl. Fig. S1** for a comparison of the delivery results using SAMPs vs. spherical magnetic particles). Each magnetized particle is a new magnetic dipole that can induce particle–particle interactions to trigger local migration and form particle chains, which also could induce scratches on cells along the particle migration paths.

Here, we demonstrate a novel, low-cost, easy-to-implement, and high-throughput platform called shape anisotropic magnetic particles (SAMPs) for macromolecule delivery into a broad range of mammalian cell types, including primary normal human dermal fibroblasts (NHDFs) and mouse cortical neurons that are difficult to transfect.

Methods and Procedures

SAMPs

The working principle of SAMPs is based on rotating shape anisotropic magnetic particles under a uniform magnetic field. Cells touching rotating magnetic particles are scratched to generate transient membrane cuts or pores for delivery. There are two unique features and major advantages of the SAMP method. First, shape anisotropic magnetization and particle rotation can be induced by a uniform magnetic field as shown in **Figure 1**. This feature provides a major advantage over conventional magnetic transfection approaches, in which a nonuniform magnetic field is required to create a field gradient to produce magnetic forces that translate micro or nano magnetic particles. Generating a constant magnetic force on magnetic particles across a large area requires the creation of a uniform "gradient" of magnetic fields across a large area, which is very difficult to achieve. In SAMPs, only a uniform magnetic field is required. Cell membrane opening is realized by rotating magnetic microparticles that scratch and cut contacting cells. When magnetic particles with anisotropic shapes are used, their easy magnetization axes will automatically align with the external magnetic field. Of note is that each of these magnetized particles is also a magnetic dipole. Magnetic dipoles can attract each other to induce local particle migration. Local particle migrations induced by particle–particle interactions, in addition to particle rotation, can also scratch and cut cell membranes. The requirement of a uniform external field in SAMPs is unique, especially for delivery across a large area (greater than a few square centimeters) since a uniform magnetic field can be easily obtained with widely available disc-shaped magnets. A second major advantage is that the SAMP approach does not require any microfabrication steps. All materials and components used in SAMPs can be easily obtained at low cost. Also, there is no need for chemical modification of the magnetic particles since SAMPs is a purely physical approach for cell membrane opening.

For SAMP delivery, the molecules of interest to be delivered were first added into the cell culture medium. Then, SAMPs were dispersed randomly and evenly onto cells at a density of 6–9 $\times$ 10^4 particles/cm^2. The culture dish was quickly placed above a disc-shaped magnet (magnet 1) for 1 s at a distance of 3–5 cm and moved away (**Fig. 2**). Magnetic field strengths were 0.039 tesla at a distance of 3 cm and 0.020 tesla at the distance of 5 cm. After 10 min of incubation at room temperature, the SAMPs were removed

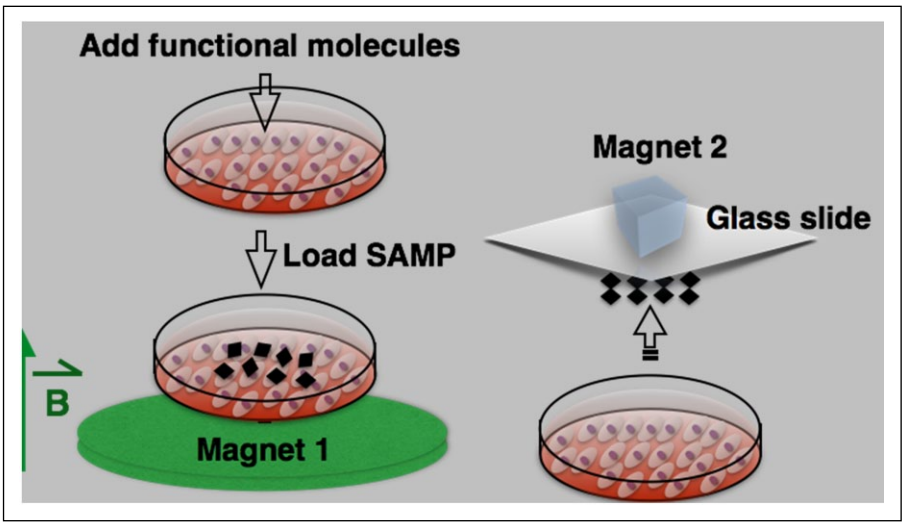

Figure 2. Procedure for intracellular delivery of functional molecules using SAMPs. Functional molecules of interest are added into the cell culture dish, SAMPs are loaded and actuated with an external magnetic field, followed by removal of SAMPs.

from the cells by another magnet (magnet 2) placed above the cultured dish. The cells were incubated with the molecules of interest for 15 min at 37 °C, washed three times with 1× PBS, pH7.4, and placed back into their culture medium.

Of note is that magnetic microparticles of 40-60 μm in diameter used in SAMPs help avoid cell engulfment by endocytosis, pinocytosis, or other mechanisms. This prevents known particle cytotoxicity issues caused by nanoparticle engulfment by cells in conventional approaches.[17,18]

Magnetic Field Distribution

Experimental measurements of the magnetic flux density of the disc magnet were compared to the theoretical results simulated by COMSOL. The magnet is a N42-graded neodymium disc (Stanford Magnets Co., Irvine, CA) and is 3 in. in diameter and ¼ in. in thickness; its surface field strength is approximately 1085 gauss. **Figure 3** compares the measured values of the normal component of magnetic flux density to those of the simulation across the magnet's surface at distances of 3 and 5 cm. A Hall probe was positioned in parallel to the surface for each measurement; thus, only the normal components of the flux were obtained.

Figure 4 illustrates the numerically simulated, corresponding magnetic field directions and flux densities at 3 and 5 cm from the disc surface, respectively. Both the simulation and experimental results show that the magnetic field strength around the center of the magnet disc is uniform and the field direction is perpendicular to the disc. For optimal SAMP delivery, micro magnetic particles are sprinkled near the center location where the magnetic field is uniform. When magnetic particles are sprinkled at locations near the edge of the magnet disc, a strong magnetic field gradient induces large magnetic forces on the particles to induce fast migration, which damages cells immediately.

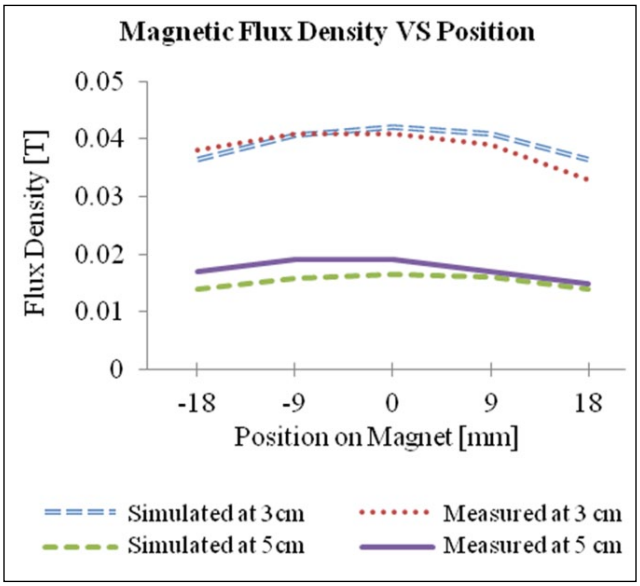

Figure 3. Measured normal components of the magnetic flux density distribution across the disc magnet used for the SAMP method at 3 and 5 cm above disc surface. The magnet's center is located at position 0 mm.

Cell Culture

HeLa cells were maintained in Dulbecco's modified Eagle's medium (DMEM, Corning) supplemented with 10% fetal bovine serum (FBS, Corning), 4.5 g/L glucose, L-glutamine, sodium pyruvate, and penicillin/streptomycin. NHDFs (Lonza, Basel, Switzerland) were cultured in Fibroblast

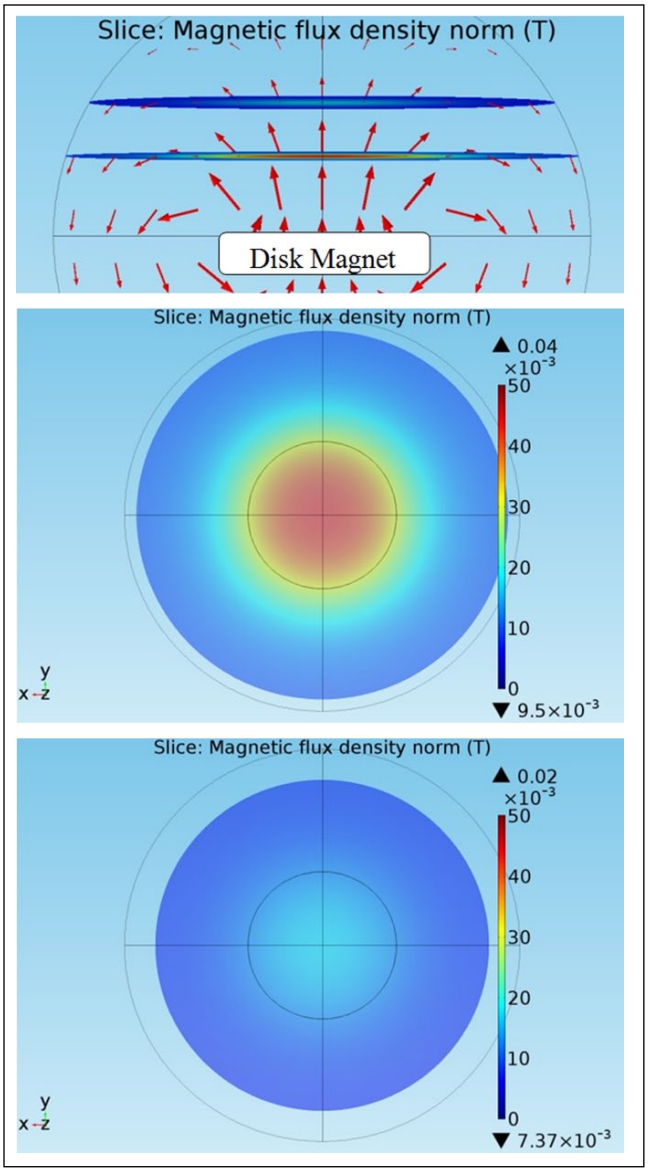

Figure 4. (**a**) Numerically simulated magnetic flux density and field direction in a cross-sectional view using COMSOL, a finite element method. The direction and length of arrows indicate the direction and strength of the magnetic field. (**b,c**) Distributions of magnetic flux density at 3 and 5 cm, respectively, above the surface of the magnet disc.

Basal Medium with hFGF-B, insulin, FBS, and gentamicin/amphotericin-B (Corning). Mouse cortical neurons were prepared from C57BL/6J mice (Jackson Laboratory, Bar Harbor, ME) on postnatal day 0 as previously described[21] and cultured in Neurobasal-A media (Life Technologies, Carlsbad, CA) supplemented with 1× B27 supplement (Life Technologies), 0.25× GlutaMAX supplement (Life Technologies), 25 µM glutamate (Sigma-Aldrich, St. Louis, MO), and 25 µM β-mercaptoethanol (Sigma-Aldrich). Before delivery, HeLa and NHDF cells were seeded in 35 mm petri dishes. Neurons were grown in 24-well multiwell plates.

Sterilization of Magnetic Particles

Magnetic particle sterilization was done by treatment of 500 mg nickel metal powder (99.9% pure, 40–60 µm in diameter, Atlantic Equipment Engineers, Upper Saddle River, NJ) with 1 mL of 75% ethanol for 30 min. One-time phosphate-buffered saline (PBS, pH 7.4, Corning) was used to wash SAMPs four times, and the SAMPs were resuspended in 1 mL 1× PBS, pH 7.4. SAMPs were stored in aliquots at 100 mg/mL in 1× PBS, pH 7.4.

Evaluation of Delivery Efficiency and Cell Viability

The delivery efficiency was calculated as the number of cells with delivered materials divided by the total number of cells. Cell viability was checked by propidium iodide (PI) staining (5 µg/mL, Invitrogen, Grand Island, NY) or, in some cases, DAPI staining (1 µg/mL, Invitrogen). PI was added to cells 10 min after the application of SAMPs and the magnetic field, incubated for 5 min, and removed. Cell viability was calculated as the number of cells without PI or DAPI staining divided by the total number of cells × 100. Fluorescence images of intracellular delivery of calcein dye and dextran particles (3 and 40 kDa), green fluorescence protein (GFP) expression, and a β-lactamase activity assay in cells were obtained by using an inverted fluorescence microscope (Axio Observer.D1m, Carl Zeiss, Oberkochen, Germany) with 10× and 40× objective lenses. Expression of lamin A/C to evaluate the efficacy of lamin A/C siRNA was also performed by immunofluorescence staining and recorded using an inverted fluorescence microscope (IX70, Olympus, Tokyo, Japan).

Results and Discussion

Efficiency and Cell Viability for Delivering Molecules of Different Sizes

To evaluate the SAMP method, three different sizes of membrane-impermeable molecules, including calcein dye (623 Da) and dextran particles (3 and 40 kDa), were delivered into HeLa cells, NHDFs, and mouse cortical neuron cells. In HeLa cells, the delivery efficiencies of calcein dye and 3 and 40 kDa dextran particles were 98.3%, 88.0%, and 62.2%, respectively (**Fig. 5**). The delivery efficiency decreased as cargo size increased since larger cargo has less time to pass through membrane pores by diffusion before they close. Similar trends were recorded for cargo delivery into NHDFs, in which the delivery efficiencies observed were 99.4%, 91.0%, and 74.6%, respectively (**Fig. 6**). Cell viability for both HeLa and NHDF cells post cargo delivery was >90% in all experiments. Of note is that stationary SAMPs without

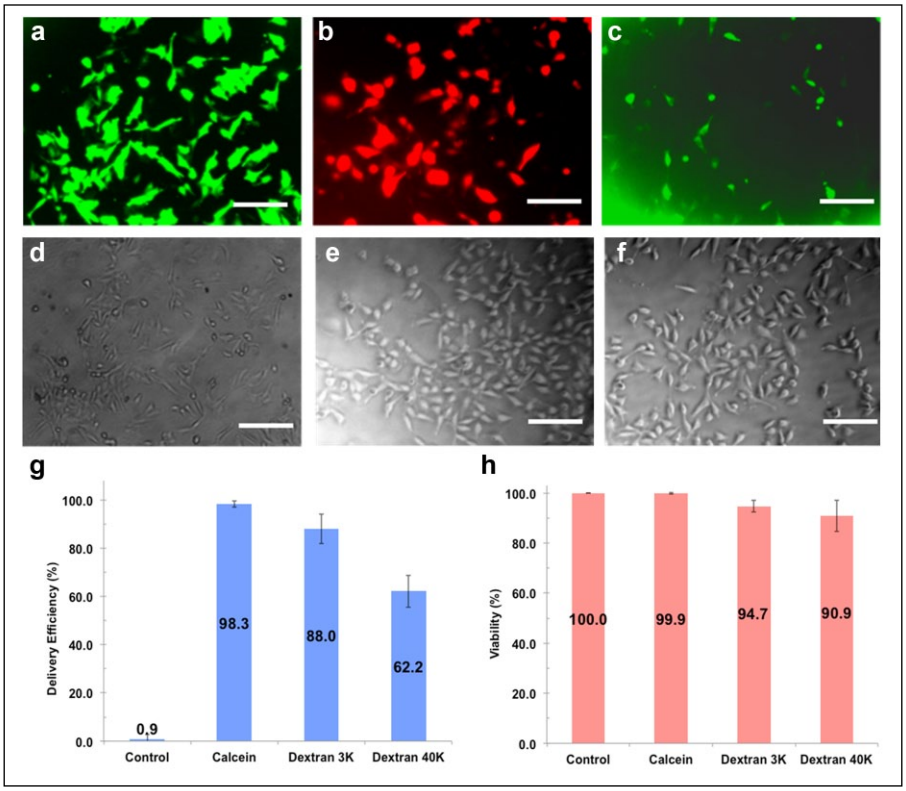

Figure 5 (a–c) Fluorescence images of HeLa cells delivered with calcein dye (0.1 mg/mL, Invitrogen), dextran 3K (1 mg/mL, tetramethylrhodamine-labeled dextran 3 kDa, Invitrogen), and dextran 40K (1 mg/mL, fluorescein-labeled dextran 40 kDa, Invitrogen) with SAMP treatment. (**d–f**) Corresponding bright field images of **a–c**. Scale bar: 200 µm. (**g,h**) Delivery efficiency and cell viability after SAMP delivery of calcein dye, dextran 3K, and dextran 40K into HeLa cells. The control group is performed by 0.1 mg/mL calcein delivery without SAMP treatment. The data are presented as a ratio of the percentage of delivered cells (cell counts in fluorescence images/cell counts in bright field images) with a total of 517 cells (control), 603 cells (calcein), 1262 cells (dextran 3K), and 525 cells (dextran 40K) from three independent repeat experiments.

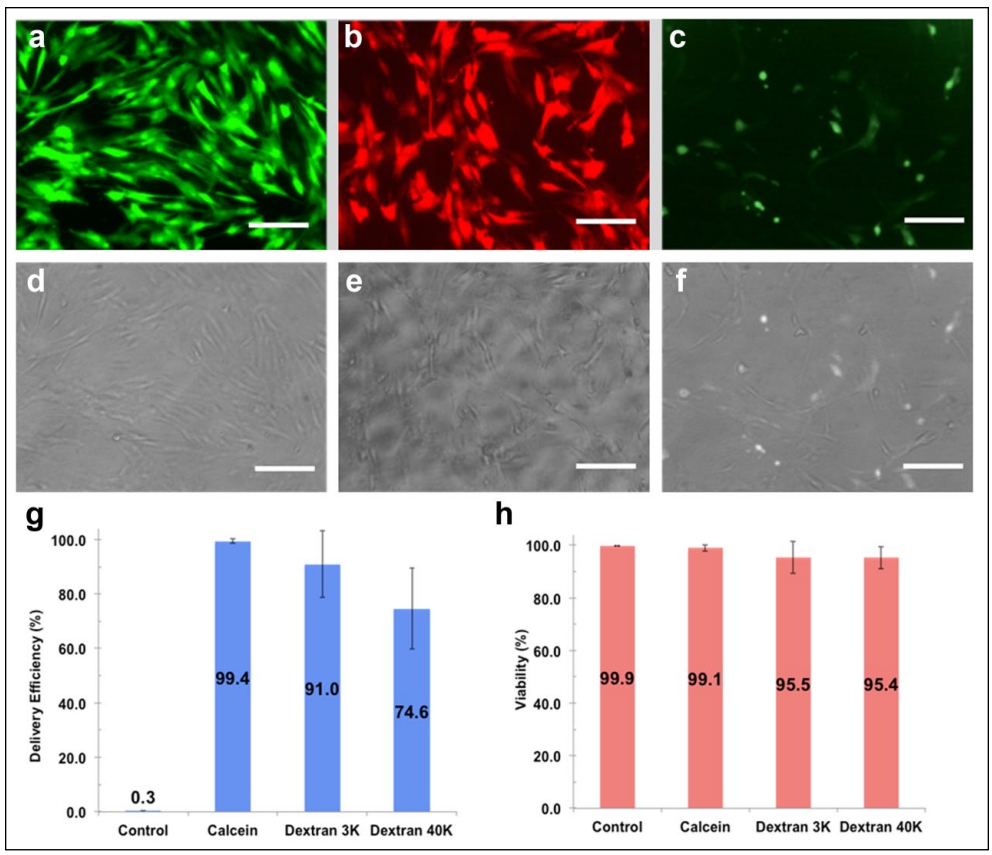

Figure 6. (**a–c**) Fluorescence images of NHDF cells after SAMP delivery of calcein dye (0.1 mg/mL), dextran 3K (1 mg/mL), and dextran 40K (1 mg/mL). (**d–f**) Corresponding bright field images are shown. Scale bar: 200 µm. (**g,h**) Delivery efficiency and cell viability after delivery into NHDF cells. The data are presented as a ratio of the percentage of delivered cells (cell counts in fluorescence images/cell counts in bright field images) with a total of 1600 cells (control), 1304 cells (calcein), 650 cells (dextran 3K), and 1052 cells (dextran 40K) from three independent repeat experiments.

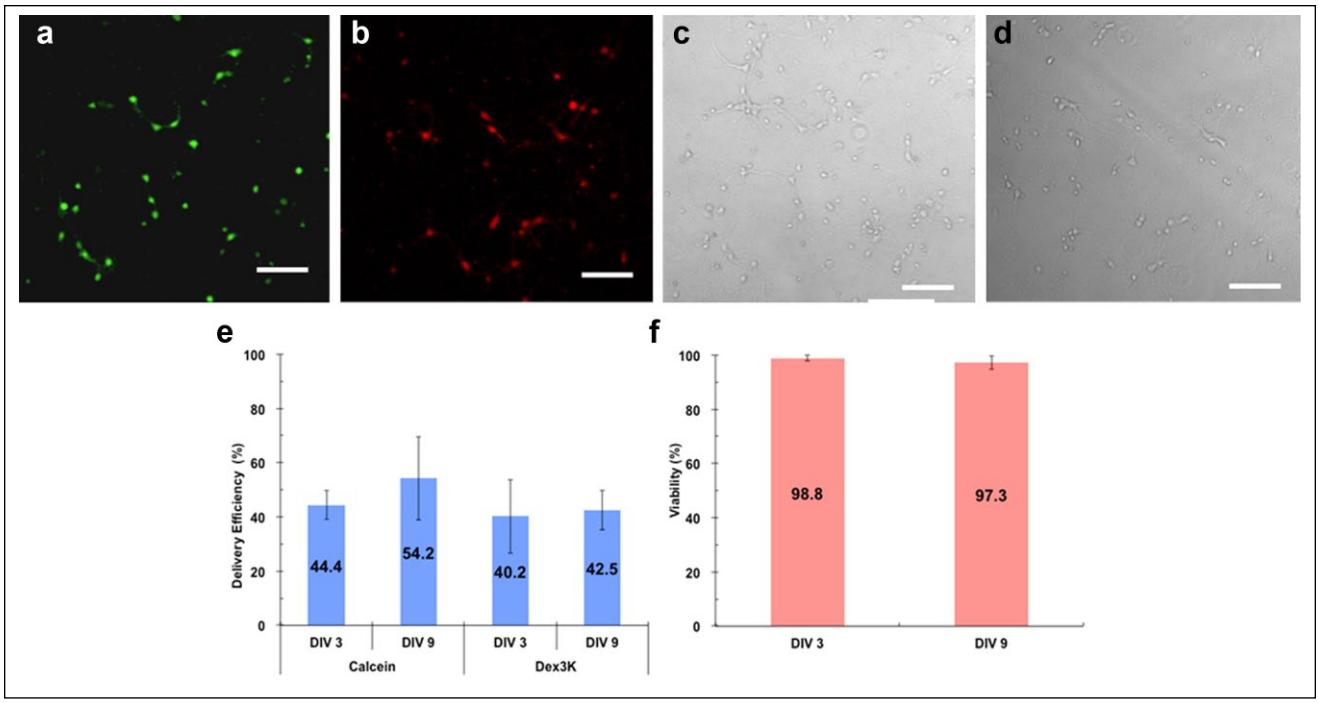

Figure 7. (**a,c**) Fluorescence and bright field images of mouse cortical neurons (9 DIV) delivered with calcein dye (0.1 mg/mL). (**b,d**) Fluorescence and bright field images of mouse cortical neurons (9 DIV) delivered with dextran 3K (1 mg/mL). Scale bar: 100 μm. (**e**) Delivery efficiencies of calcein dye and dextran 3K into neurons on DIV 3 and 9 with SAMP treatment, respectively. (**f**) Neuron viabilities on DIV 3 and 9 after SAMP delivery. The data are presented as a ratio of the percentage of delivered cells (cell counts in fluorescence images/cell counts in bright field images) with a total of 710 cells for Calcein-DIV3, 662 cells for Dex3K-DIV3, 1140 cells for Calcein-DIV9, 1017 cells for Dex3K-DIV9, 1447 cells for Viability-DIV3, and 1140 cells for Viability-DIV9.

magnetic field–induced rotation have negligible effects on delivery efficiency and viability (data not shown).

Intracellular delivery of macromolecules into postmitotic cells currently remains challenging. Therefore, we tested SAMP delivery efficiency in primary cultured neurons that are postmitotic. Using the SAMP method, calcein dye was delivered into 44.4% of mouse cortical neurons that were cultured 3 days in vitro (DIV) after preparation from mouse brain at postnatal day 0, and 3 kDa dextran was delivered into 40.2% of neurons at the same age (**Fig. 7**). Similar delivery efficiencies of 54.2% for calcein dye and 42.5% for 3 kDa dextran particles were achieved for more mature neurons at the age of DIV 9. Moreover, >97% cell viability was recorded for neurons at both ages post-SAMP delivery (**Fig. 7e**).

Delivery of Plasmids and siRNAs

We delivered a liposome-coated GFP expression plasmid (pEGFP-N1, 4.7 kb) using SAMPs. Approximately 72.2% of NHDF cells expressed GFP 48 h after delivery on the SAMP platform. This is a fivefold higher efficiency than NHDF cell delivery by liposome encapsulation only (13.3%) (**Fig. 8a,b,g**). Protein expression from introduced plasmid DNA using lipofection techniques is typically low, with significant cytotoxicity in many primary cell types.[12,22] Therefore, the SAMP platform could facilitate the delivery of functional plasmids into primary cells.

Variable efficiencies for intracellular delivery of siRNAs into different cell types have been reported.[23] Therefore, a method for efficient delivery of siRNAs into cells would be important for basic studies and possibly translational applications. With SAMPs, 95.4% of HeLa cells were transduced by lipofectamine-encapsulated siRNA against lamin A/C. A reduction of lamin A/C protein from 90.6% to 7.0% was observed by immunocytochemistry, validating SAMP delivery of siRNA into HeLa cells (**Fig. 8c–f,h**).

Delivery of β-Lactamase and Enzyme Cascade Reaction

Enzyme therapeutics is a promising and growing field in medicine because of catalytic activity and specificity of the approach. Protein and enzyme deliveries are challenging with other platforms due to the large size of the delivered cargo and the need to preserve functions postdelivery. The bacterial enzyme β-lactamase was delivered by SAMPs into NHDF cells and delivery efficiency and functionality

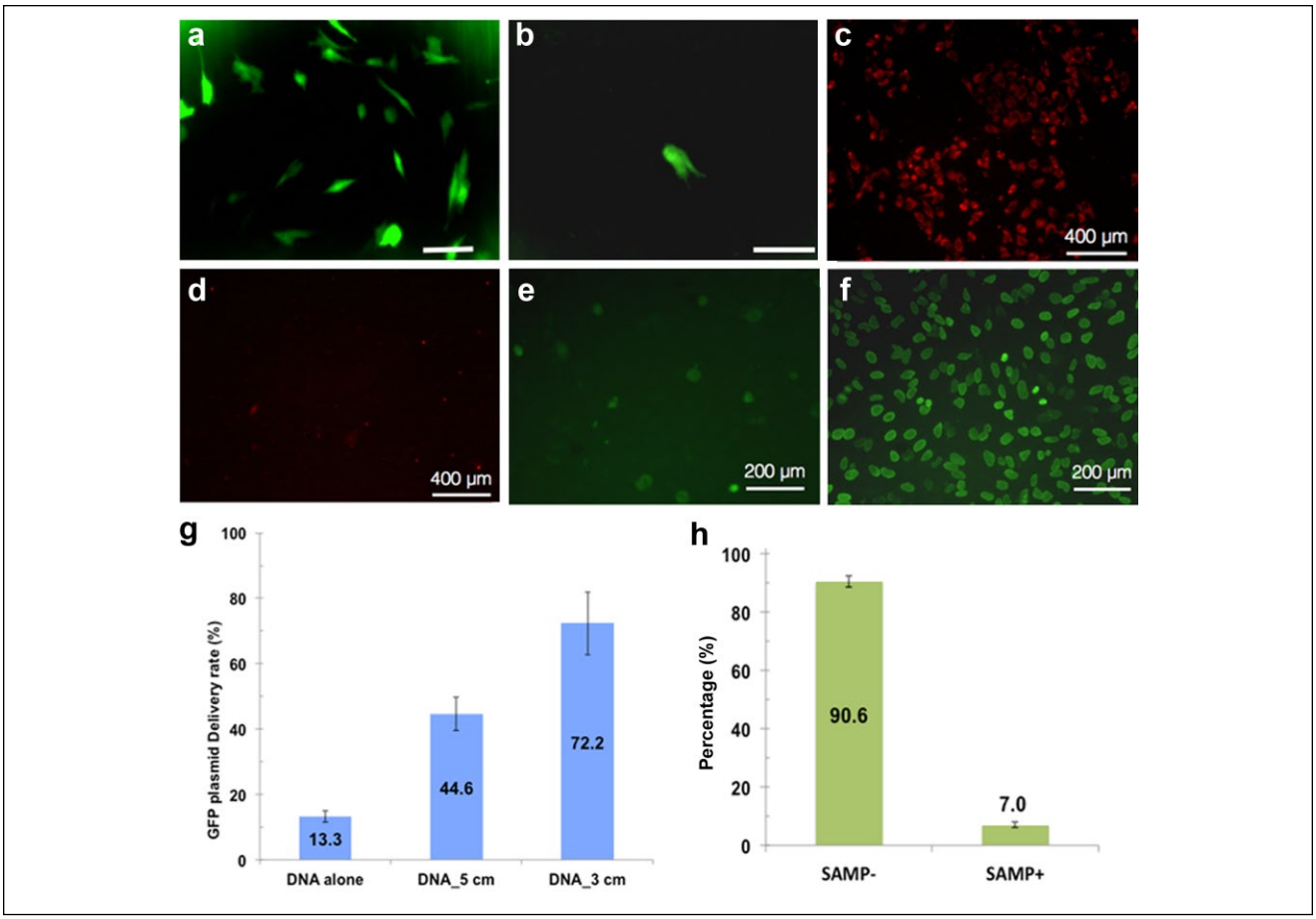

Figure 8. Intracellular delivery of functional nucleic acid molecules: GFP plasmids and siRNA. (**a**) Fluorescence image of GFP-expressed NHDF cells after SAMP delivery. The distance of Ni powders and bottom magnet is 3 cm. The GFP plasmid (6 ng/μL) is pretreated with lipofectamine. Scale bar: 200 μm (**b**) The control group of GFP-expressed NHDF cells incubated with lipofectamine-pretreated GFP plasmid without SAMP-assisted delivery. Scale bar: 200 μm (**c**) Fluorescence image of lamin A/C siRNA-delivered HeLa cells with SAMPs. The distance between the Ni powders and the bottom magnet is 3 cm. The lamin A/C siRNA (50 nM) is pretreated with lipofectamine and labeled with fluorescence dye, DY-547. (**d**) Control group of HeLa cells incubated with lipofectamine-pretreated lamin A/C siRNA. (**e**) Fluorescence image of immunocytochemistry staining with lamin A/C monoclonal antibody on HeLa cells after SAMP delivery of lamin A/C siRNA. (**f**) Fluorescence immunochemistry staining of Hela cells without SAMP-assisted delivery of lamin A/C. Cells after SAMP delivery of lamin A/C siRNA shows much weaker fluorescence signals due to the silencing of the expression of lamin protein by siRNA. (**g**) Comparison of efficiency of SAMP delivery of GFP plasmid into NHDF cells with the magnet disc positioned at 5 and 3 cm from the cells, and the case without SAMPs. (**h**) Comparison of percentage of HeLa cells expressing lamin A/C protein after delivery of siRNA molecules with SAMP treatment (SAMP+) and without SAMPs (SAMP–). For cells after SAMP delivery of siRNA, the expression of lamin A/C protein is significantly suppressed to 7%.

assessed by incubation with the membrane-permeant substrate CCF4-AM, a lipophilic, esterified form of the CCF4 substrate, which allows it to readily enter cells, in postdelivery NHDF cells. CCF4-AM is naturally converted into CCF4 by endogenous esterases and retained in the cytosol in NHDFs. CCF4 is a fluorescence resonance energy transfer (FRET) substrate that consists of a cephalosporin core linking 7-hydroxycoumarin to fluorescein. In the absence of β-lactamase activity, emission of a green fluorescence signal at 530 nm from CCF4 is observed by FRET with excitation at 408 nm (**Fig. 9a–c**). In the presence of exogenous β-lactamase activity, cleavage of CCF4 disrupts FRET, resulting in emission of a blue fluorescence signal at 460 nm. We observed that delivery of β-lactamase (10 or 50 units/mL) into NHDF cells resulted in the conversion of a green fluorescence signal to blue fluorescence (**Fig. d–f**). Cells placed at 3 cm (stronger magnetic field) above the magnet show a higher delivery efficiency than at 5 cm (weaker magnetic field), and in both cases showed a high cell viability of >98% after SAMP treatment. Three concentrations of β-lactamase (10, 50, and 100 IU/mL) were SAMPs delivered for comparison. The highest delivery efficiency, 89.9%, was achieved at a concentration of 100 IU/mL (**Fig. 9h**). These results indicate that SAMP delivery

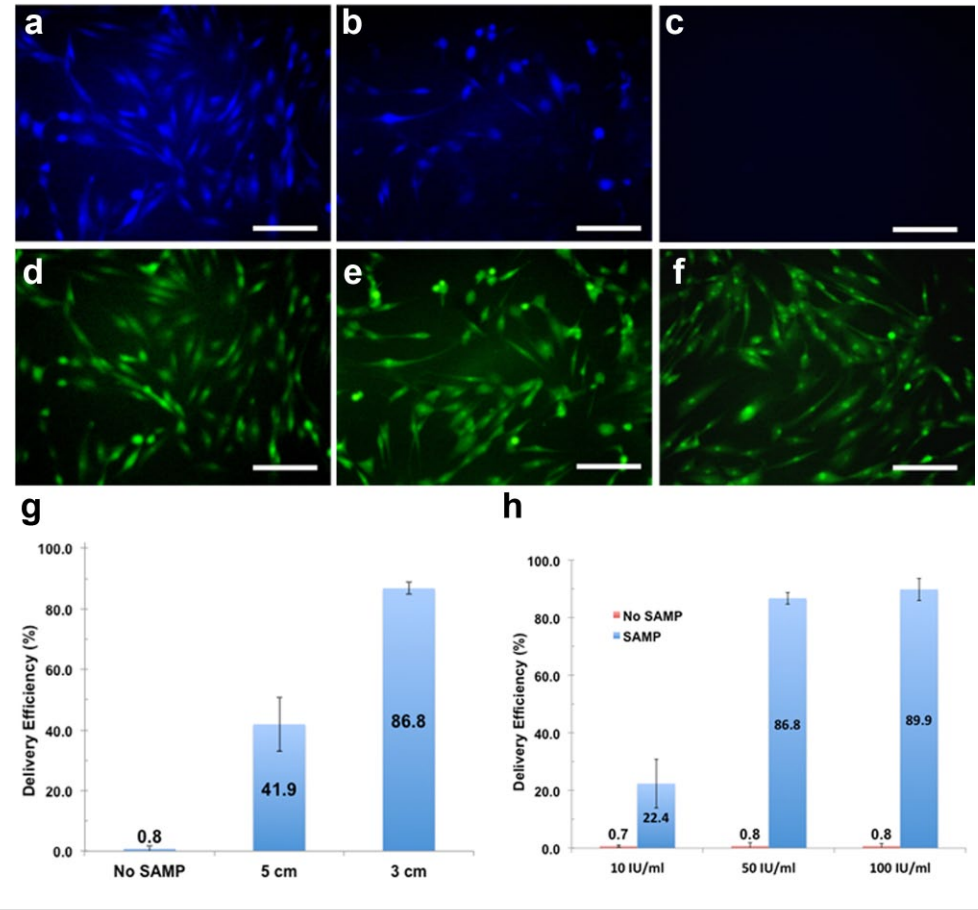

Figure 9. SAMP-delivered β-lactamase enzyme shows catalytic function in NHDF cells. (**a,d**) SAMP delivery of β-lactamase at 50 IU/mL with the magnet disc at 3 cm. CCF4 (green fluorescence) is generated by cytosolic esterase in NHDF cells. If exogenous β-lactamase was successfully delivered with catalytic functions preserved, it cleaves the CCF4 molecule and generates blue fluorescence. The fluorescence images are taken at 4 h after delivery. Scale bar: 200 μm. (**b,e**) SAMP delivery of β-lactamase at 10 IU/mL with the magnet disc at 3 cm. (**c,f**) β-Lactamase (50 IU/mL) without SAMP treatment. (**g**) Study of the effect of magnetic field strength and the delivery efficiency of β-lactamase (50 IU/mL). Cell viabilities in this study are all above 98%. (**h**) Concentration effect on delivery efficiency using SAMPs and without. Higher delivered efficiency is observed with increasing the concentration of β-lactamase. However, without SAMPs, the β-lactamase delivery is low even at high concentration.

of the exogenous β-lactamase into NHDFs is highly efficient with the catalytic enzyme activity maintained.

Conclusions

We demonstrated an easy-to-use, low-cost, and high-throughput SAMP method for high-efficiency intracellular delivery. SAMP delivery is purely physical and less cell type dependent. It is realized by rotating micron-sized, anisotropic-shaped magnetic particles that scratch and induce cell membrane cuts for cargo to pass through into the cytosol. SAMPs is a batch mode delivery approach, and each batch can deliver ~40,000 cells in 10 min in the current proof-of-concept demonstration. The throughput is linearly proportional to the area of a uniform magnetic field created by the magnet. Higher throughput up to a few million cells per batch can potentially be achieved by using a larger-sized disc magnet. Through properly controlled magnetic particle density, size, and magnetic field strength, SAMP delivery provides high cell viability and high efficiency delivery of a wide range of small and medium-sized molecules, including calcein dye, 3 and 40 kDa dextran particles, a GFP plasmid, an siRNA, and an enzyme (β-lactamase), into multiple cell types, including postmitotic mouse cortical neurons. The current SAMP approach was optimized for adherent cells. Cell adhesion to a substrate provides an anchoring balance force to allow membrane cuts to form during the particle scratching process. Without such adhesion, a cell will be pushed away before a membrane cut is formed. Extending the application of SAMP delivery to nonadherent

cells will require a substrate that can hold cells through other mechanisms, such as mechanical confinement or adhesion-promoting materials.

Declaration of Conflicting Interests

The authors declared no potential conflicts of interest with respect to the research, authorship, and/or publication of this article.

Funding

The authors disclosed receipt of the following financial support for the research, authorship, and/or publication of this article: This work is supported by a University of California Discovery Biotechnology award (178517); National Institutes of Health grants AI065359, GM114188, CA185189, and EB014456; U.S. Air Force Office of Scientific Research award FA9550-15-1-0406; and NanoCav, LLC (Culver City, CA). This work is also funded by NSF CBET-1404080.

References

1. Estrada, L. H.; Chu, S.; Champion, J. A. Protein Nanoparticles for Intracellular Delivery of Therapeutic Enzymes. *J. Pharm. Sci*. **2014**, *103* (6), 1863–1871.
2. Chang, F. P.; Chen, Y. P.; Mou, C. Y. Intracellular Implantation of Enzymes in Hollow Silica Nanospheres for Protein Therapy: Cascade System of Superoxide Dismutase and Catalase. *Small* **2014**, *10* (22), 4785–4795.
3. Luo, D.; Saltzman, W. M. Synthetic DNA Delivery Systems. *Nat. Biotechnol*. **2000**, *18* (1), 33–37.
4. Dahlman, J. E.; Barnes, C.; Khan, O. F.; et al. In Vivo Endothelial siRNA Delivery Using Polymeric Nanoparticles with Low Molecular Weight. *Nat. Nanotechnol*. **2014**, *9* (8), 648–655.
5. Forbes, D. C.; Peppas, N. A. Polycationic Nanoparticles for siRNA Delivery: Comparing ARGET ATRP and UV-Initiated Formulations. *ACS Nano* **2014**, *8*(3), 2908–2917.
6. Shen, J.; Wu, X.; Lee, Y.; et al. Porous Silicon Microparticles for Delivery of siRNA Therapeutics. *J. Visualized Exp*. **2015**, *95*, 52075.
7. Yin, H.; Kanasty, R. L.; Eltoukhy, A. A.; et al. Non-Viral Vectors for Gene-Based Therapy. *Nat. Rev. Genet*. **2014**, *15* (8), 541–555.
8. Xu, J.; Teslaa, T.; Wu, T.-H.; et al. Nanoblade Delivery and Incorporation of Quantum Dot Conjugates into Tubulin Networks in Live Cells. *Nano Lett*. **2012**, *12* (11), 5669–5672.
9. Bai, M.; Bai, X.; Wang, L. Real-Time Fluorescence Tracking of Gene Delivery via Multifunctional Nanocomposites. *Anal. Chem*. **2014**, *86* (22), 11196–11202.
10. Dobrovolskaia, M. A.; McNeil, S. E. Strategy for Selecting Nanotechnology Carriers to Overcome Immunological and Hematological Toxicities Challenging Clinical Translation of Nucleic Acid-Based Therapeutics. *Expert Opin. Drug Deliv*. **2015**, *12* (7), 1163–1175.
11. Liu, Y.; Wang, D.-A. Viral Vector-Mediated Transgenic Cell Therapy in Regenerative Medicine: Safety of the Process. *Expert Opin. Biol. Ther*. **2015**, *15* (4), 559–567.
12. Movahedi, F.; Hu, R. G.; Becker, D. L.; et al. Stimuli-Responsive Liposomes for the Delivery of Nucleic Acid Therapeutics. *Nanomedicine* **2015**, *11* (6), 1575–1584.
13. Deng, X.; Zheng, N.; Song, Z.; et al. Trigger-Responsive, Fast-Degradable Poly(β-Amino Ester)s for Enhanced DNA Unpackaging and Reduced Toxicity. *Biomaterials* **2014**, *35* (18), 5006–5015.
14. Wu, M.; Zhao, D.; Wei, Z.; et al. Method for Electric Parametric Characterization and Optimization of Electroporation on a Chip. *Anal. Chem*. **2013**, *85* (9), 4483–4491.
15. Zong, S.; Wang, Z.; Chen, H.; et al. Surface Enhanced Raman Scattering Traceable and Glutathione Responsive Nanocarrier for the Intracellular Drug Delivery. *Anal. Chem*. **2013**, *85* (4), 2223–2230.
16. Na, Y.-R.; Kim, S. Y.; Gaublomme, J. T.; et al. Probing Enzymatic Activity Inside Living Cells Using a Nanowire–Cell "Sandwich" Assay. *Nano Lett*. **2012**, *13* (1), 153–158.
17. Singh, S. P.; Rahman, M.; Murty, U.; et al. Comparative Study of Genotoxicity and Tissue Distribution of Nano and Micron Sized Iron Oxide in Rats after Acute Oral Treatment. *Toxicol. Appl. Pharmacol*. **2013**, *266* (1), 56–66.
18. Colombo, M.; Carregal-Romero, S.; Casula, M. F. Biological Applications of Magnetic Nanoparticles. *Chem. Soc. Rev*. **2012**, *41* (11), 4306–4334.
19. Wu, T.-H.; Teslaa, T.; Kalim, S.; et al. Photothermal Nanoblade for Large Cargo Delivery into Mammalian Cells. *Anal. Chem*. **2011**, *83*, 1321–1327.
20. Wu, Y.-C.; Wu, T.-H.; Clemens, D. L.; et al. Massively Parallel Delivery of Large Cargo into Mammalian Cells with Light Pulses. *Nat. Methods* **2015**, *12*, 439–444.
21. Ho, V. M.; Dallalzadeh, L. O.; Karathanasis, N.; et al. GluA2 mRNA Distribution and Regulation by miR-124 in Hippocampal Neurons. *Mol. Cell. Neurosci*. **2014**, *61*, 1–12.
22. Chen, M.; Li, W.; Fan, J.; et al. An Efficient Gene Transduction System for Studying Gene Function in Primary Human Dermal Fibroblasts and Epidermal Keratinocytes. *Clin. Exp. Dermatol*. **2003**, *28* (2), 193–199.
23. Dalby, B.; Cates, S.; Harris, A.; et al. Advanced Transfection with Lipofectamine 2000 Reagent: Primary Neurons, siRNA, and High-Throughput Applications. *Methods* **2004**, *33* (2), 95–103.